

Linking Optical SPOT and Unmanned Aerial Vehicle data for a rapid biomass estimation in a Forest-savanna Transitional Zone of Ghana

Pabi Opoku^{1*}, Adu-Asare Alvin¹, Ofori Benjamin D¹

¹*Institute for Environment and Sanitation Studies (IESS), Box LG 209, University of Ghana, Accra*

*Corresponding Author: opabi@staff.ug.edu.gh

Abstract

The direct estimation of biomass using remote sensing technologies, such as LiDAR, RaDAR and Stereo Data is limited in utility, since it does not allow for historical analysis of biomass dynamics far back in time due to their recency in development. This study links Unmanned Aerial Vehicle (UAV)-measured tree height and optical SPOT image reflectance in a mathematical model for a quick and less expensive indirect biomass estimation, and the possibility of historical analysis using the earliest captured optical data. SPOT 6/7 images were used to map land-use/cover patterns. A Phantom 4 drone images were used for height and crown width estimation. A stepwise regression analysis was conducted to establish a relationship between SPOT 6/7 channels and the UAV-generated tree heights. The linear model was used to convert the reflectance values of SPOT images into tree heights, and in turn used for crown width estimation. The estimated tree height and crown width images were used to estimate biomass using an allometric equation. There was no statistically significant difference between UAV and manual tree height measurements. UAV-estimated tree height predicted 88.0% of crown width. Regressing the tree height on the SPOT bands yielded an R^2 of 66.0%. It is recommended that further studies be conducted to improve on the accuracy of estimation. It is hoped this would facilitate a quick biomass estimation and long term historical dynamics.

Introduction

Biomass estimation is an important element for biomass stock accounting, exploitation dynamics and conversion into carbon (Mate, Johansson, and Siteo 2014, De-Miguel, Mehtätalo, and Durkaya 2014). Above ground woody vegetation constitutes enormous proportion of global carbon sink, consequently important for global carbon sink management programmes (Dawson et al. 2011; Mi Sun and Yeo-Chang 2013). In the prevailing context of rapid dynamics in biomass stocks, it is essential to harness available innovative technologies for rapid and cheaper assessment for monitoring the trends in biomass stocks for management. Current use of remote sensing technologies, such as LiDAR, RaDAR and Stereo Data, for direct biomass estimation is limited in utility, since it does not allow historical analysis of biomass dynamics far back in time due to their recency in development. This study

links UAV and optical SPOT images in a mathematical model for a quick and less expensive indirect biomass estimation, and the possibility of historical analysis using other optical data archive captured close to the beginning of the emergence of satellite remote sensing technologies.

One of the fundamental tools for a non-destructive assessment of woody biomass is allometric equations (Mendoza-Ponce and Galicia 2010; Fernández-Landa, Navarro, Condes, Algeet-Abarquero, and Marchamalo 2017). Measurements on tree components are incorporated in allometric equations for biomass estimation (Brown, 2002; Chave et al., 2005). Diameter at breast height and weight are identified to produce more accurate estimates (Bacciniet al., 2012; Rutishauser et al., 2013). However, they require field-based measurements, which is more time consuming, hence, less suitable for rapid and large-scale assessment. Height is a

critical component for many equations, and a key indicator of tree growth, and used to depicting life history of growth (King & Clark, 2011; Banin et al., 2012). It has long been used to assess and estimate timber resources (Avery and Burkhart, 2011), and recently forest biomass and carbon stocks (Feldpausch et al. 2012). Height-biomass models have also been used for mangrove biomass and carbon estimations (Fatoyinbo, Simard, Washington-Allen, and Shugart 2008; Fatoyinbo and Simard 2013), and tropical forest (Fernández-Landa, Navarro, Condes, Algeet-Abarquero, and Marchamalo 2017). However, manual methods for height measurements are limited in application to smaller areas (Korning and Thomsen 1994; Goodwind 2004). They are labour intensive, expensive and time-consuming, hence, unsuitable for rapid assessment.

Remote sensing-based innovative applications in vegetation assessment have demonstrated improved success rates (Lagomasino, Fatoyinbo, Lee, Feliciano, Trettin, and Simard 2016; Pargal et al., 2017). However, the earliest captured images are optical, which cannot be used for direct plant components measurements for biomass estimation. Thus, inference of plant biomass from optical satellite imagery has been through a proxy of vegetation cover which does not accurately represent biomass (Amanor and Pabi 2007; Pabi 2007; Meroni, Rembold, Verstraete, Gomme, Schucknecht, and Beye 2014). The emergence of stereo satellite remote sensing, LiDAR and RaDAR technologies have enabled direct height and biomass estimation (Ahmed, Siqueira, and Hensley, 2013; Allouis, Durrieu, Vega, and Coueron, 2013). However, they are more expensive than optical images, and mostly targeted at limited areas of high commercial

value. Historically, these technologies of recent origin, with limited data accumulation, has a limitation for temporal studies. They are also expensive and operationally sophisticated (Angelo, Lehner, Krauss, Hoja, and De, 2008). The use of UAV for peaceful applications in recent times has gained popularity (Colomina and Molina, 2014). These can be deployed to provide three dimensional (3D) images to estimate tree heights (Lim et al. 2015). Unlike satellite and other manned remote sensing platforms, these are very cheap and simple to operate. Drones have provided relatively inexpensive alternatives for capturing very high resolution ground data (Colomina, Blázquez, Molina, Parés, and Wis 2008; Eisenbeiss 2009). The use of UAV has also been used in the direct measurements of tree heights (Lim et al., 2015; Zarco-Tejada, Diaz-Varela, Angileri, and Loudjani, 2014).

With the limitations of using the extensive historical accumulated optical data for direct biomass estimation, and the limited accumulated data capable of direct biomass estimation, the obvious question was how to leverage the synergy of these technologies for a rapid and indirect cost-effective estimation of biomass, and historical analysis? Specifically, is it possible to establish a mathematical relationship between optical image signals and direct measurements of tree parameters by UAV for biomass assessment on landscapes? It is posited that spectral signatures of trees vary with growth due to crown structural property and physiological changes (Brando, Goetz, Baccini, Nepstad, Beck, and Christman 2010; Bradley et al. 2011; Samanta et al. 2012). This study develops a predictive model for tree height using UAV-tree height measurements and the reflectance of SPOT optical image channels, and uses the established model for

height prediction from optical channels as the predictor variables. It incorporates the predicted height and crown width images in an allometric equation for biomass estimation.

The study was conducted in the Kintampo area which is located within the forest-savanna transition of Ghana, which is a naturally unstable and heterogeneous ecosystem. The zone is subjected to a multiplicity of land uses, including charcoal production. The availability and dynamics of wood resources in the area has been a subject of debate. The search for evidence of aboveground (AG) biomass stocks dynamics to inform objective discourse and policy for management has been based on inferences from vegetation cover and greening indicators using optical satellite data, which do not make accurate representation of biomass (Pabi 2007; Amanor and Pabi, 2007). The study reports on a methodology that could be used for generating information on actual biomass, rather than rely on inferences from vegetation cover. It also has the potential to examine the historical dynamics in future, and to inform discourse and policy on rapidly changing landscapes. The rest of the paper presents the methodology through conclusion.

Materials and Methods

Study Area

Location and size

The study area is located in the Kintampo North and South districts (figure 1) in the Brong Ahafo Region of Ghana, and bound by longitudes 1°20'W and 2°1'E and latitude 8°45'N and 7°40'N. The two districts together have a total land area of 6621.34 Km² (Ghana Statistical Service, 2014). It is within the Volta Basin and the Southern Voltaian Plateau. The Voltaian Basin consist of flat-bedded rocks and is extremely plain with rolling and rise and falls on the land surface with an altitude of between 60-150 metres above sea level. Many of the rivers in the area flow into the Black Volta, a major tributary of the Volta river.

The annual rainfall ranges from 1,400mm-1,800mm, and occurs in two seasons: from May to July and from September to October. Due to the transitional nature of the area, the two peaks are sometimes indistinguishable. The mean temperatures of the area range between 26.5 °C and 27.2 °C annually, with the dry season experiencing the relative humidity ranging from 75% - 80 % during the

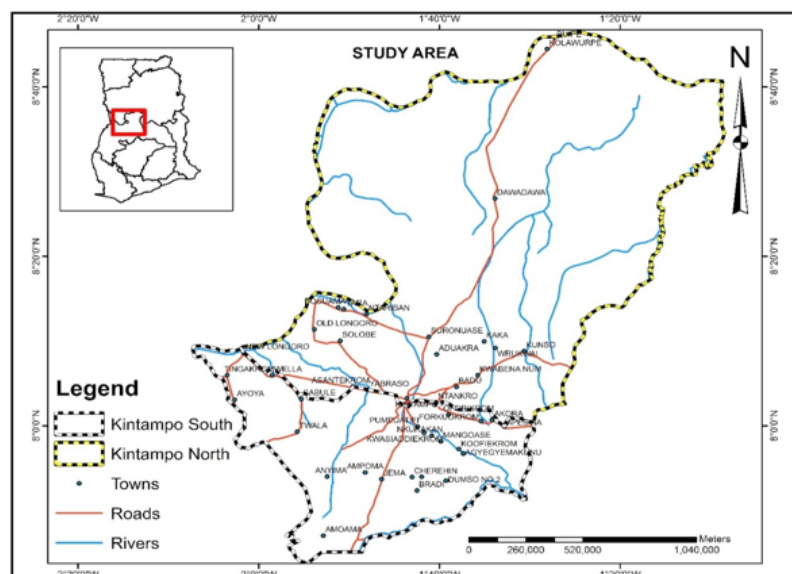


Fig 1 Study Area

dry season, and from 90% - 95% in the rainy season.

Vegetation and land use

The vegetation consists of woodland, guinea savanna and dry semi-deciduous mosaics (Forestry Commission, 2012), with these patches significantly affected by land uses. Land use activities include logging, hunting, agriculture of both traditional and mechanized practices, livestock rearing, and charcoal production. These activities coupled with bush burning are perceived to be the main drivers of vegetation change (Asante, 2014). The main crops are cowpea, maize, groundnut, and bambara bean. Yam dominates in the savanna areas, with maize dominating the areas bordering the semi-deciduous forest. Recently, tree cash crops such as mango and cashew are becoming more common, and key sources of income.

Methods

Satellite imagery acquisition

A six (6) meter resolution SPOT 6/7 images were acquired from GeoAirbus Defense and Space in France. These images were acquired for two sites: one situated in the more savanna

area and the other in the more deciduous section. The images acquired were captured on November 09, 2016, and January 01, 2016 for the south and north sites respectively. These dates were considered comparable since they were captured in the same anniversary period (dry season), and also for the fact that temporal change analysis was not intended. All the images acquired were composed of four bands; red, blue, green and NIR, and came in a UTM Zone 30N coordinate system and WGS 84 datum.

Image processing and classification

Radiometric corrections were performed on the satellite images to remove distortions from the images. Image enhancement was performed using the interactive stretching tool in ENVI 5.0 on bands 1, 4, 2. Both supervised and unsupervised classification were conducted. The unsupervised classification was carried out using the Iterative Self Organizing Data Analysis (ISODATA classification). A minimum of 7 and a maximum of 15 class thresholds were defined. After the initial unsupervised classification, and reclassification to eight (8) classes, it was imported to ArcMap. Polygons shapes for the classes were created in ArcMap, and

TABLE 1
Classification scheme used for the study

Cover Type	Description
Cropped farmlands	Lands with annual crops such as cassava, maize, yam on isolated or treeless land and cowpea
Bareland/ Cleared Farms	These are non-vegetated lands which are bare due to thin topsoil or cleared for farming. Others had mounds for yam cultivation.
Built up	These were physically built areas such as buildings, roads, etc.
Short Fallow	Abandoned farmed lands harvested of crops, left uncultivated for about 2-5 years. There were saplings of trees shrubs with an average height of 3 meters. Isolated tree canopy cover is mostly less than 20%.
Long Fallow	These mature fallows left uncultivated for more than six years. The trees are relatively taller than those on short fallows, with an average tree height of 8 meters. Where thickets are present, they are difficult to penetrate. Their canopy cover is usually between 60-80%, with wider openings having thicker bushes and grass cover.

TABLE 1 *cont*
Classification scheme used for the study

Cover Type	Description
Grassland	These are lands with predominant grass cover and herbs, with widely opened trees and shrubs. These are found on permanent cropped lands, savanna mosaics with thin top soils underlain with gravels and rocks or slopes.
Dense woodland/Forest	This is very matured vegetation cover type dominated by trees, and left uncultivated for about 10 or more years. They may form part of forest mosaics or woodland vegetation, usually located on low lying areas, along water bodies or on good soils with good supply of water. The canopy cover is mostly greater than 70%. The trees heights are mostly greater than 15 meters with some reaching as high as 24 m or more

converted to kml files. These were then imported to Google earth pro to assist with field verification in ground truthing for field measurements and identify training areas for the supervised classification. A Global Positioning System (GPS) (Garmin) was used to record the coordinates of the training samples of the land cover types. The spectral signatures of these training data were used to compute training statistics for each land cover class, and supervised classification conducted using the Maximum likelihood algorithm. The classification scheme adopted the classes in table 1.

Samples of vegetation cover types were studied for tree heights, photographed and geolocated with GPS during ground truthing for detailed characterization and assessing the accuracy of the classification. These points were different from those used as training data

during the supervised classification process. These points were used to create region of interests (ROIs). A confusion matrix was then performed in ENVI 5.0.

Tree Height Measurement

Unmanned Aerial Vehicle and pre-flight operations

Phantom 4 propeller UAV was used. It has a vertical flight limit of 6000m, and could be controlled remotely within a 5 km radius. The drone is equipped with a 12-megapixel digital camera and produces images in the green, red, and blue spectral bands. The field of view of the camera is 94° and an electronic shutter speed of 1/8000 s. The camera is being held by a gimbal which has a controllable range of -90 ° to 30°. The Phantom 4 is also equipped with an onboard Global Navigation Satellite

TABLE 2
Flight Summary

Flight	No of Images	Duration	Cover Type	Location
1 st	22	2mins	Dense woodland	Mansie
2 nd	58	3mins	Short Fallow	Yabraso
3 rd	462	24mins	Long Fallow	Sronuase
4 th	146	5mins	Dense woodland	Naabia
5 th	401	14mins	Long Fallow/short fallow	Tandene

Systems (GNSS) to regulate and manipulate the flight and to provide positions.

Pre-flying sessions were conducted before each flight to identify safe areas for takeoff and landing in order to avoid or reduce damages to the UAV. Areas of interest were identified with suitable flying conditions to avoid significant shifts of the UAV from its flying path. Vertical and horizontal calibration of the UAV was also performed at this stage to correct instrumental errors. Image capturing process was operated from an android tablet with a mission control software named pix4DCapture. All the flight paths were planned in the mission control software prior to flying. The double grid flight path was used to enable a stereo data capture for the generation of 3D models. An end overlap of 70% and a side overlap of 80% was applied, and flight altitude of 60-80 meters since more close-up images were required for high resolution 3D models. The camera was tilted vertically downwards to enable 3D construction. The images were captured in WGS 84 30N coordinate system. Flight and summary of images captured from the various land use land cover types with the duration taken by the UAV to cover the cover type is shown in table 2.

UAV image processing for DSM, DEM and CHM generation

Images from UAV were processed using Agisoft Photoscan software. The images were imported into the software and used to produce a mesh, followed by a dense point cloud production. PhotoScan calculates the depth information for each camera which is put together into a single dense point cloud, making it almost as dense as the LiDAR point cloud. The dense point clouds were classified into ground point clouds and above ground

point clouds.

This was exported as a LAS file into ArcGIS 10.4.1. The point clouds were then converted into a multipoint file to make processing and manipulation faster. A Digital Elevation Model (DEM), which is height of the bare ground was generated from the ground point cloud. A Digital Surface Model (DSM) which is made up of heights of trees and the bare ground was also generated from the above ground point clouds. The generation of the DEM and the DSM allowed the generation of Canopy Height Model (CHM), which is the height of trees on the surface of the earth. This was achieved by subtracting the DEM from the DSM.

Ground measurements of tree heights and

$$CHM = DSM - DEM \dots\dots\dots \text{Equation (1)}$$

UAV accuracy assessment

A comprehensive field measurement was undertaken to evaluate the accuracy of tree height measurement with the UAV. Tree heights of different height categories were measured on the field with the use of a well-calibrated stick and a clinometer. A total of forty-two (42) trees were measured manually. The actual heights of trees were measured three times and the averages calculated. The corresponding geographic coordinates of the measured trees were also recorded with GPS with an accuracy of between $\pm 2-2.30\text{m}$. These points were then overlaid on the tree heights generated from the UAV, and the points extracted in ArcGIS. A t-test was performed to confirm if there was a statistically significant difference between the means of tree heights measured on the field and tree heights generated from the UAV.

Relationship between UAV heights and SPOT

Image reflectance values

The CHM generated was geometrically corrected using image to image registration to ensure that the pixels in both the tree heights generated and the various bands within the satellite images were all at the same place using the georeferencing tool in ArcGIS 10.4.1. Points were randomly placed on the tree heights images. A total of 699 pixel points were selected. Height values were extracted as point shapes. These were overlaid on all the four bands of the SPOT images, and the corresponding reflectance values extracted. The attribute table was exported as a STATA readable format for further analysis.

A multicollinearity test was carried out to determine the level of association between the SPOT bands. Shapiro-Wilk test of normality was used to test for goodness of fit of the variables used. A stepwise regression was conducted to determine the most statistically significant predictors which are necessary for the establishing the relationship (model) and how each of predicting variable was contributing to the model (Lopez-Serrano *et al.* 2015). The UAV-generated height (actual) was regressed on the SPOT channel reflectance values.

Tree Crown Diameter and Height Relationship

Tree crown diameter was estimated from the UAV generated images. The images were converted into dense point clouds which

depicted the shape of trees on the field. This made it easy for depiction of distinct tree crown samples for width measurement using Agisoft Photoscan software. The corresponding tree heights were also measured to allow an establishment of association between tree height and crown diameter, using crown width as a response variable and height as a predictor variable. The predictive model was used to derive tree crown width from the tree heights derived from the SPOT satellite images.

Biomass Estimation Modelling

The multiple regression model developed was used to predict height (response variable) values from the optical SPOT channels (independent variables). The height raster data was used for biomass estimation. The Allometric equation adopted was developed by Jucker *et al* (2017), as shown in equation (1). The equation was chosen because it makes use of the tree height and crown diameter parameter for estimating aboveground biomass of a tree. The equation was used to convert the heights values generated from the SPOT channels into biomass using the raster calculator in ArcGIS 10.4.1

Where, AGB represents Above Ground

$$AGB = 0.016 * (H * CD)^{2.013} * EXP^{\frac{0.204^2}{2}} \dots \text{Equation (2)}$$

Biomass, H represents tree heights, CD is Crown Diameter.

In order to quantify the amount of biomass

TABLE 3
Summary statistics of predictor variables (bands) used for regression analysis

Variables	No.	Minimum	Maximum	Mean	Std. Deviation
Tree Heights	699	2.12m	26.08m	9.27	5.20487
Band 1	699	697	1129	837.28	56.0978
Band2	699	857	1081	977.14	41.18936
Band 3	699	758	917	842.87	29.22098
Band 4	699	2477	3249	2872.29	139.88993

available for each class on which charcoal is being exploited, the land use land cover classes were vectorised in ENVI 5.0. the vector file was then overlaid on the biomass derived from the satellite images and the biomass extracted using ArcGIS 10.4.1.

Results

The overall accuracy of the classification is 90.05% with a corresponding Kappa coefficient of 0.8820. Table 4 shows the

on the landscape, with other wood extractive activities less obvious. The classified SPOT images (figure 2), with the amount of different classes presented in table 4.

UAV tree height measurement and accuracy assessment

The t-test indicated statistically no significant difference ($p > 0.05$) between tree heights measured from by the UAV and actual tree heights by the manual method. The mean

TABLE 4
Land area covered by the various land use cover types

Cover Types	Area (m ²)	Area (Km ²)	Area (Ha)	Percentage (%)
Grassland	116410000	116.41	11641	10.38
Short Fallow	456580000	456.58	45658	40.70
Water	2400000	2.40	240	0.21
Cropland	24880000	24.88	2488	2.22
Bareland/cleared Farmed land	205370000	205.37	20537	18.31
Dense woodland	113810000	113.81	11381	10.15
Long fallow	167300000	167.30	16730	14.91
Built up	34980000	34.98	3498	3.12
Total	1121730000	1,121.73	112173	100.00

amount of different categories of the different land use and land cover types. The fallows constituted a major portion of the vegetation cover, with the dense woodland forming a smaller percentage of the total land cover. Farming appeared widespread human activity

tree heights by the UAV and one by the stick and clinometer measurement were 7.84m and 8.48m respectively. Sample of vegetation point clouds, DSM and DEM are displayed in figures 3, 4 and 5 respectively.

SPOT reflectance and UAV-Generated Tree

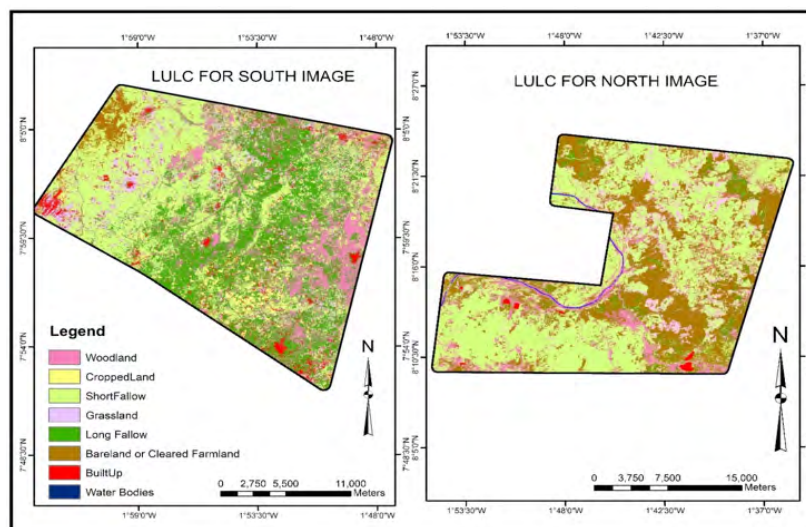


Fig 2 Land use land cover for south (Left) and north (Right) images

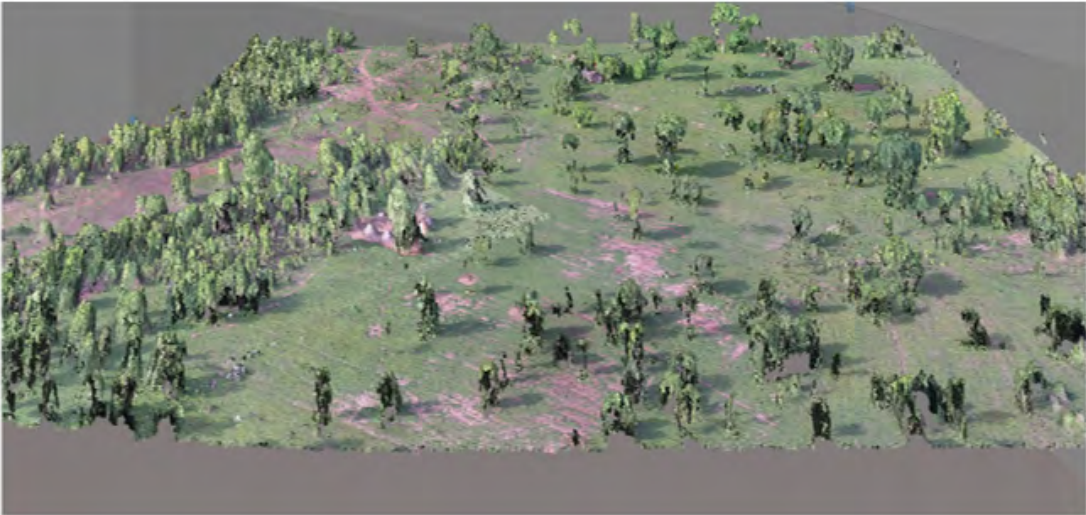


Fig 3 Sample of Point Clouds generated from the UAV

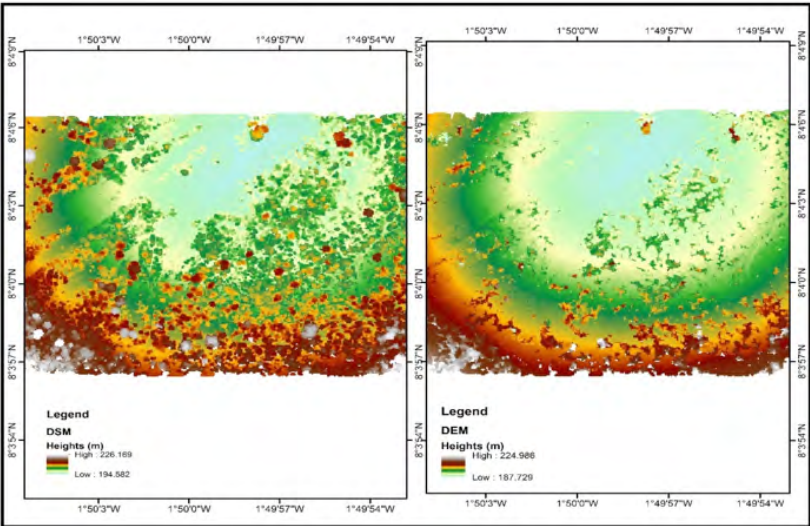


Fig 4 DSM and DEM samples from UAV data

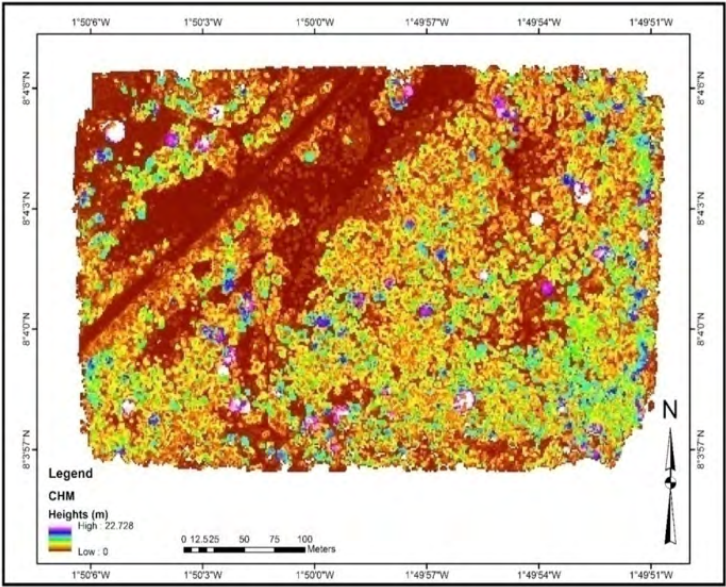


Fig 5 Tree Height from UAV data

Heights relationship

The relationship between the tree heights and the reflectance of SPOT channels are displayed in figure 6. All the channels of the satellite data displayed negative relationship but strong association, with the exception of band 4 that showed no association. They also had moderate coefficient of determination. The test of normality indicated that the samples used for establishing the relationship (model) were of good fit. The Variance Inflation Factor

(VIF) for all the predictor variables (SPOT bands) were under 10. This suggests that there was no existence of multicollinearity. The equations derived from the relationship is shown in table 5 and 6. The model fit between the predictor variables and the response (tree height) were significant ($p < 0.05$). The changes in R^2 for the stepwise regression were very low (table 6).

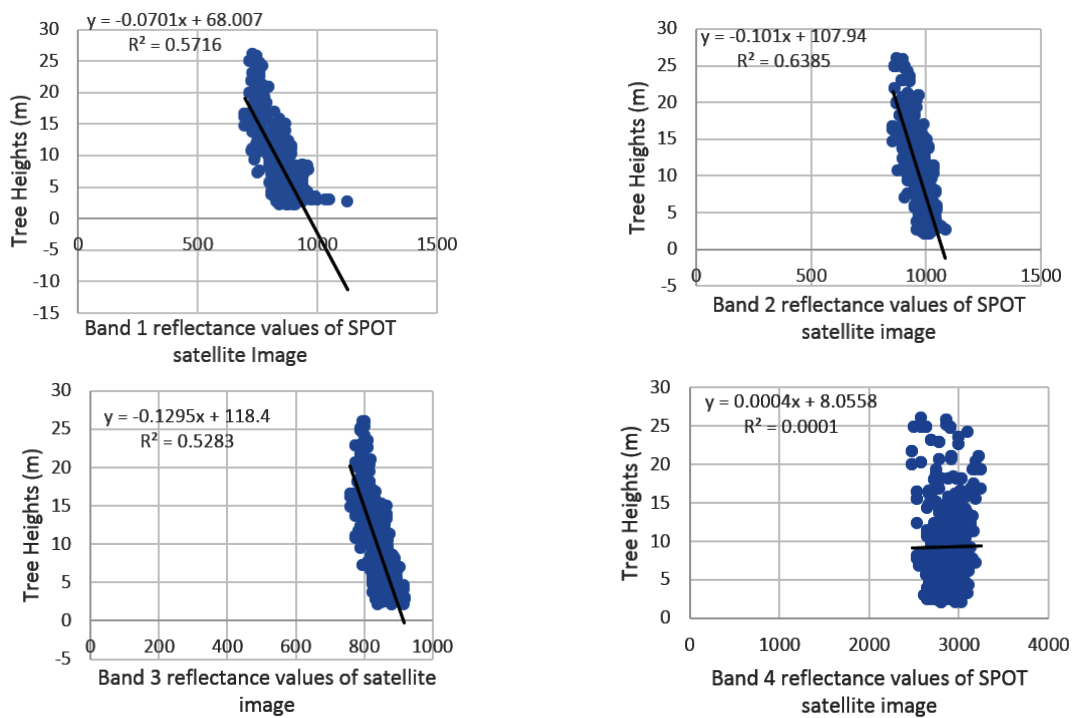


Fig 6 Relationship between tree heights and bands reflectance values of SPOT satellite image

TABLE 5
Coefficients of UAV tree heights and SPOT reflectance values model

	Model	Coefficients	Std. Error	F	P-value
1	(Constant)	107.940	2.814		
	Band2	-0.101	0.003	1231.147	0.000
2	(Constant)	117.892	3.359		
	Band2	-0.079	0.005		
	Band3	-0.037	0.007	652.254	0.000
3	(Constant)	110.278	4.293		
	Band2	-0.083	0.005		
	Band3	-0.032	0.007	441.864	0.000
	Band4	0.002	0.001		

Durbin-Watson= 1.369

TABLE 6
Regression models between UAV tree heights and SPOT reflectance values

Model	Regression Model	R	R Square	R Square Change
1	H= 107.94-0.101(Band 2)	.799	0.64	0.639
2	H= 117.892-0.079(Band 2)-0.037(Band 3)	.808	0.65	0.014
3	H= 110.278-0.083(Band 2)-0.032(Band 3)+0.002(Band 4)	.810	0.66	0.004

Relationship between Tree Heights and Crown Diameter

Crown diameter of trees are presented in figure 7. The result indicated that there is a strong linear relationship between tree heights and crown diameter as depicted by a high R² value based on 51 tree samples. The predictive model developed from this association was used to convert the tree heights derived from the satellite images to tree crown diameter.

Biomass Estimation

Figures 8 and 9 present tree heights generated from the SPOT images. The heights ranged between 3-24m for the southern site, and 3-22m for the northern image. Figures 10

and 11 presents the crown diameter for the SPOT images. Tree crown diameter ranged 2-9m for southern site, and 2-8m for northern site. Biomass derived from the SPOT satellite images based on the allometric equation are shown in figures 12 and 13. The total amount of biomass and their distribution among dense woodlands, short fallows and long fallows are shown in table 7. The results indicated that the highest concentration of biomass was found in the dense woodlands, that is, 13.66 Mg/ha. This was followed by long and short fallow respectively. However, the total amount of biomass for each category of land cover was highest in short fallows, followed by long fallow (table 7).

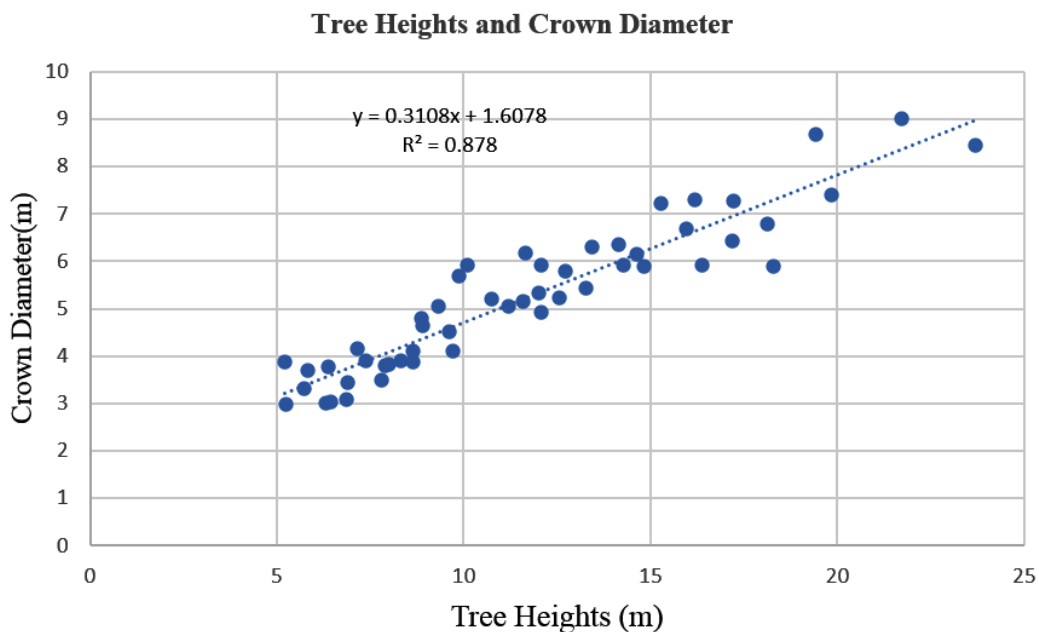


Fig 7 Relationship between tree heights and crown diameter

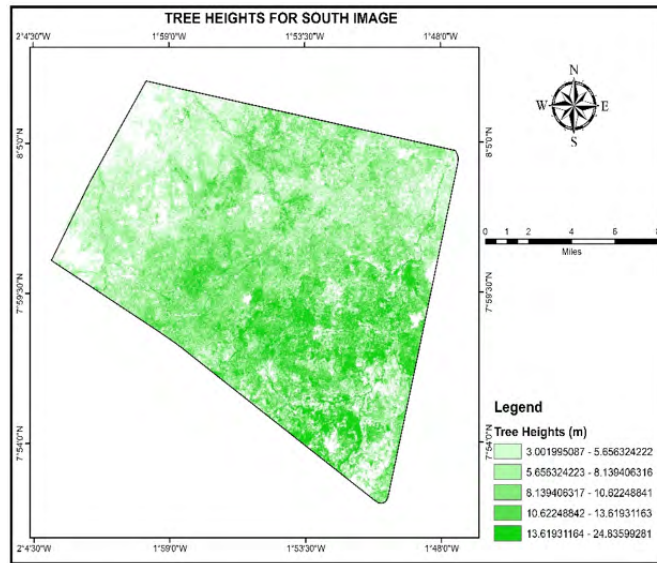


Fig 8 Tree height for the southern site

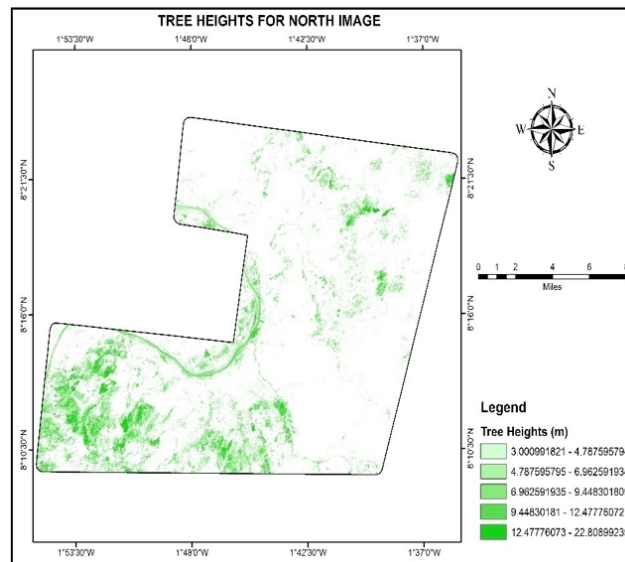


Fig 9 Tree height for the Northern Site

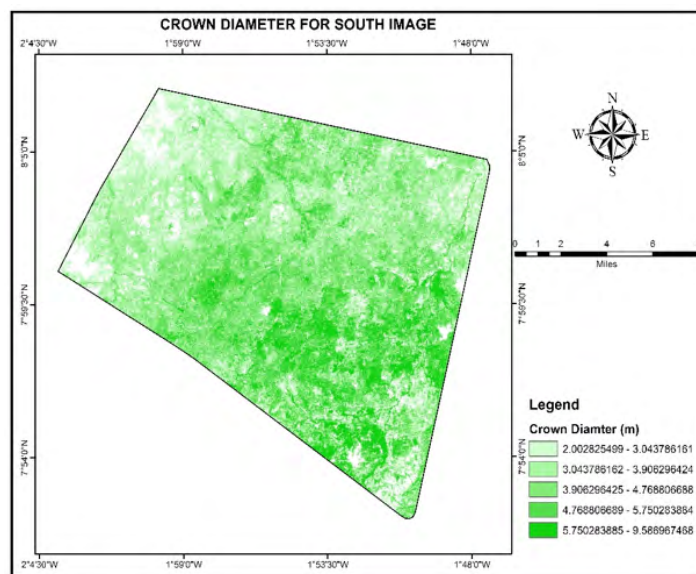


Fig 10 Tree crown width derived from south satellite image

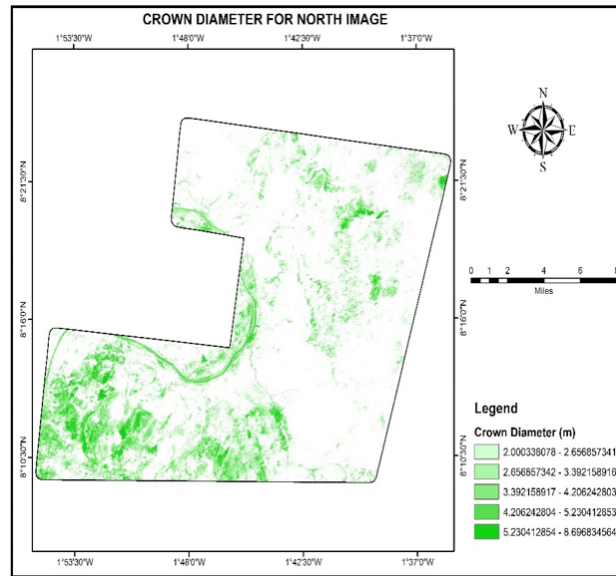


Fig 11 Crown Diameter from north satellite image

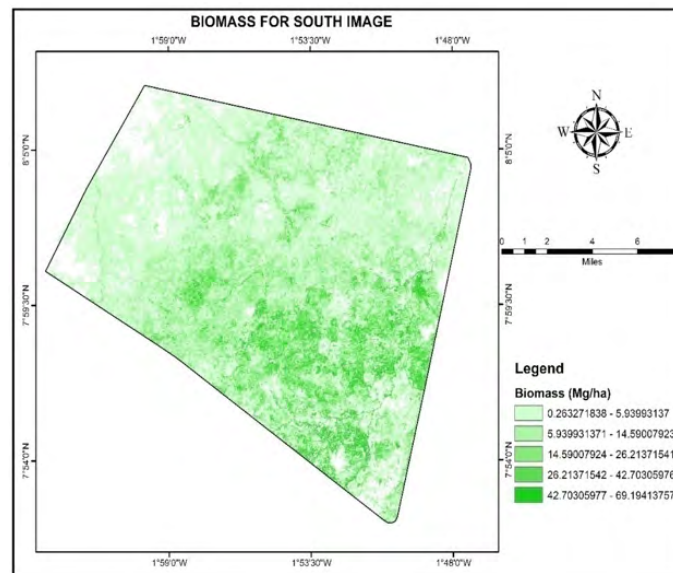


Fig 12 Biomass derived from south satellite image

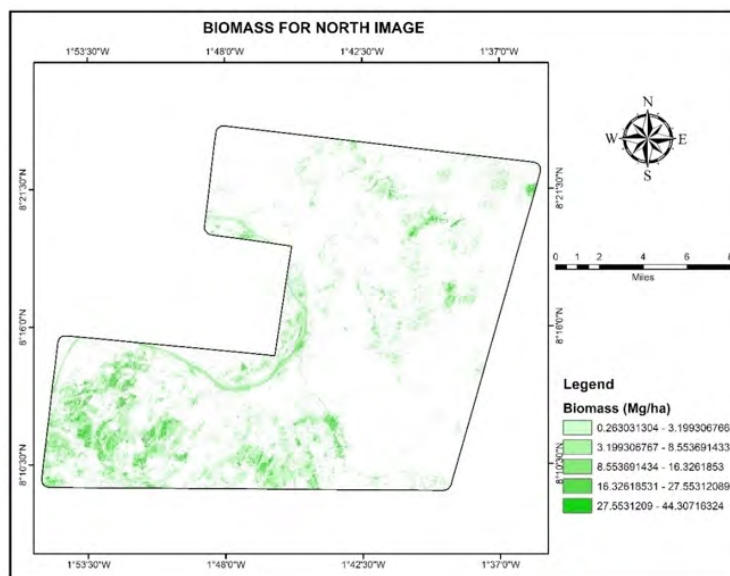


Fig 13 Biomass distribution derived from north image

TABLE 7
Biomass Distribution among cover types

Cover Type	Sum (Mg)	Biomass Density (Mg/ha)	Mean
Long Fallow	158449.175	9.470960849	41.92994
Short Fallow	98934.37647	2.166857428	21.97795
Dense Woodland	155572.4905	13.66949218	87.30605

Discussion

Land Use, Land Cover and Biomass

The SPOT 6/7 images used for this study enabled a good distinction between the various land cover types. For instance, the separation of long fallow, short fallow, and dense woodland with an overall accuracy of 90 percent and a kappa coefficient of 0.88 respectively gives an indication of the high capacity of the SPOT image to separate different objects. This conforms with other studies conducted using SPOT images (Conrad, Fritsch, Zeidler, Rücker, and Dech 2010; Zhang, Zhou, Chen, and Ma 2011).

The land use land cover types identified in the study reflect the dominant land uses, and the inherent nature of the vegetation in the area, that is mosaics of both savanna and forest (Pabi, 2007). The presence of farms, long fallows, short fallows and grassland indicate the level of exploitation of the natural landscape. The high proportion of fallows shows a practice of both shifting cultivation, with a high level of intensification and intensification (permanent) cultivation, and extractive exploitation of wood resources for charcoal production and other uses (DEAR, 2005). The presence of low amounts of dense woodlands could be due to the increasing demand for fertile land for farming and wood extraction. Continuous use of land with attendant fertility loss pushes farmers into matured fertile lands Yelsang(2013). The

area covered by bare land and grassland is, especially, towards the northern part of the study area is due to the savannah nature of the area: characterised by slender trees and large grass that whither during the dry season, and the dominantly mechanized farming practice in the area.

UAV tree-height measurement accuracy and relationship with SPOT reflectance

From the results, it is obvious that tree heights generated from the UAV provided a fair representation of actual tree heights. The t-test result indicates no statistically significant difference between the tree heights generated from the UAV and the actual tree heights taken from the ground ($p < 0.05$). The coefficient of determination, R^2 of 86.5% indicates that practically no other factors influence the variations in the actual values except some random errors. Thus, drone height is a very good determinant of actual tree height. A study conducted by Zarco-Tejada et al. (2014) who estimated tree heights with UAV recorded R^2 of 83.0% and a root mean square error of 35cm. Previous studies also obtained similar results (Bendig et al., 2014; Lisein, Pierrot-Deseilligny, Bonnet, and Lejeune, 2013). A research conducted by Karpina, Jarzabek-Rychard, Tymków, and Borkowski (2016) generated an extremely low error of 5cm. These limited variations could be attributed to the altitude of flight, human errors, specificity

of in-built accuracy of UAV. These results suggest height measurements by the drone is highly accurate.

From the tree height model, it could be seen that the bands used for the model have strong association with the tree heights generated from the UAV. The strength of the relationship between the reflectance values of the SPOT bands and the tree heights generated from the UAV vary. The stepwise regression method used for the generation of model eliminated band 1 from the model as it may have contributed insignificantly to the model variation. Theoretically, band 1 is heavily absorbed by vegetation, hence limiting in reflective vegetative signals relevant for vegetation studies. The inverse relation between bands two and three, on the one hand and tree height on the other could be attributed to the high level of reflective vegetative information content in band 2. Also, band 3 has been used for vegetation water stress studies (Zhao and Running, 2010; Forzieri, Feyen, Cescatti, and Vivoni, 2014). Band 4 acquires information in the NIR portion of the electromagnetic spectrum. This is usually used to study and analyse vegetation vigor and structure. Some studies have used this band in combination with band 1 to generate normalised differential vegetation index (NDVI) (Foody, Boyd, and Cutler, 2003; Gonzalez-Alonso, Merino-De-Miguel, Roldan-Zamarron, Garcia-Gigorro, and Cuevas, 2006).

The rule of thumb for checking the non-existence of multicollinearity among the predictor variables suggest that the variance inflation factor should not be more than 10 (Kleinbaum, Kupper, and Muller, 1988). The predictor variables passed this test as the VIF values were below 10. The model also passed for autocorrelation test as the Durbin-Watson

value of 1.369 is within the rule of thumb range of 1 to 2. The height model R^2 of 0.66 based on the three bands suggests that 66% of the total variation in tree heights can be explained by the model. It implies that other factors influence tree heights measurements. Sampling errors and those due to remote sensing imagery may partly contribute to this unexplained portion of height variation.

Biomass Estimation

The result of the biomass estimation obtained (figures 9 and 10) is expected, as it logically follows from the range of values recorded from the DSM and the DEM. The biomass estimated is about 66% ($R^2=66\%$) of the total expected amount of actual biomass, which is consistent with a study where UAV measurements were used to predict biomass (Dandois and Ellis, 2013). It must be noted, however, that biomass estimation in this study is indirectly derived from UAV values. The order of the density of biomass distribution follows an expected natural order, that is, woodland through short fallows (table 7). Of the total amount of estimated biomass, fallows constituted the highest source of biomass followed by the woodland. Among these cover types, short fallow had most of the biomass followed by long fallow and then dense woodland. This could be attributed to the large area covered by short and long fallows, though the tree heights on this cover types are relatively shorter than dense woodland.

Conclusion

The use of UAV imagery provides an effective assessment of tree height and crown width, as indicated in this and previous studies (Zarco-Tejada *et al.* 2014, Karpina *et al.* 2016). The

main purpose of the study was to explore the possibility of establishing a linkage between long historically accumulated optical satellite image and UAV data could for applications in temporal biomass change analysis. This study has demonstrated a significant relation between data captured from UAV and SPOT satellite platform. Theoretically, this should be anticipated since they capture some common spectral information from the electromagnetic spectrum. The limitation in the use of UAV sensor in this study is that they do not capture data from all channels of satellite sensors, hence relevant information content may not be available for analysis. There could be improvement if UAV sensors with high spectral resolutions are used.

The use of satellites sensors with high spatial resolution could improve the estimation of biomass since it will improve selection of distinct homogenous samples, whilst reducing mixed pixels. This will be very relevant in the applications of large-scale rapid biomass assessment of woody resources for monitoring on landscapes of high heterogeneity due to a diversity of land uses and vegetation cover of different plant types and sizes, as was the case of the Kintampo area. Intensive farming and charcoal burning result in rapid and complex vegetation dynamics. Different cover types have different biomass: the total amount partly depends on the coverage of available cover. Further studies with the use of other optical satellite data with high spatial and spectral resolutions, with long historical achieved data should be explored. It is hoped that the proportion of biomass explained by the model equation would significantly increased to a higher proportion if the above suggestions are duly considered in future studies.

Aknowledgement

We acknowledge funding for the: Access and Exclusion Along the Charcoal Commodity Chain project provided by DANIDA, Denmark. We declare that there is no conflict of interest attached to this paper.

References

- Ahmed, R., Siqueira, P., & Hensley, S.** (2013). A study of forest biomass estimates from Lidar in the northern temperate forests of New England. *Remote Sensing of Environment*, **130**, 121–135.
- Allouis, T., Durrieu, S., Vega, C., & Coueron, P.** (2013). Stem volume and above-ground biomass estimation of individual pine trees from LiDAR data: Contribution of full-waveform signals". *IEEE Journal of Sel. Top. Application of Earth Observation Remote Sensing*, **6**, 924–934.
- Amanor, K. S., & Pabi, O.** (2007). Space, time, rethoric and agricultural change in the transition zone of Ghana. *Human Ecology*, **(35)**, 51–67.
- Angelo, P., Lehner, M., Krauss, T., Hoja, D., & De, P. R.** (2008). Towards automated dem generation from high resolution stereo satellite images. *The International Archives of the Photogrammetry, Remote Sensing and Spatial Information Sciences, International Society for Photogrammetry and Remote Sensing*, **37(B4)**, 1137–1342.
- Asante, W.** (2014). *Operational Guidance and Standards for National and Subnational REDD + Programs in Ghana*.
- Avery, T. E., & Burkhart, H.** (2011). *Forest Measurements* (5th ed.). New York: McGraw-Hill.

- Baccini, A. G. S. J., Goetz, S. J., Walker, W. S., Laporte, N. T., Sun, M., Sulla-Menashe, D., & Samanta, S.** (2012). Estimated carbon dioxide emissions from tropical deforestation improved by carbon-density maps. *Nature Climate Change*, **2(3)**, 182–185.
- Banin, L., Feldpausch, T. R., Phillips, O. L., Baker, T. R., Lloyd, J., Affum-Baffoe, K., & Davies, S.** (2012). What controls tropical forest architecture? Testing environmental, structural and floristic drivers. *Global Ecology and Biogeography*, **21(12)**, 1179–1190.
- Bendig, J., Bolten, A., Bennertz, S., Broscheit, J., Eichfuss, S., & Bareth, G.** (2014). Estimating biomass of barley using crop surface models (CSMs) derived from UAV-based RGB imaging. *Remote Sensing*, **6(11)**, 10395–10412.
- Bradley, A.V., Gerard, F.F., Barbier, N., Weedon, G.P., Anderson, L.O., Huntingford, C., Aragao, L.E.O.C, Zelazowski, P., & Arai, E.** (2011). Relationships between phenology, radiation and precipitation in the Amazon region. *Global Change Biology* **17**: 2245–22, .60.
- Brando, P., M. Goetz, S.J., Baccini, A., Nepstad, D.C., Beck, P.S.A., & Christman M.C.** (2010). Seasonal and interannual variability of climate and vegetation indices across the Amazon. *Proceedings of the National Academy of Sciences, USA* **107**: 14685–14690.
- Brown, S.** (2002). Measuring Carbon in Forests: Current status and future challenges. *Environmental Pollution*, **116(3)**, 363–372.
- Chave, J., Andalo, C., Brown, S., Cairns, M. A., Chambers, J. Q., Eamus, D., ... & Yamakura, T.** (2005). Tree allometry and improved estimation of carbon stocks and balance in tropical forests. *Oecologia*, **145(1)**, 87–99.
- Colomina, I., & Molina, P.** (2014). Unmanned aerial systems for photogrammetry and remote sensing: A review. *ISPRS Journal of Photogrammetry and Remote Sensing*, **92**, 79–97.
- Colomina, I., Blázquez, M., Molina, P., Parés, M. E., & Wis, M.** (2008). Towards a new paradigm for high-resolution low-cost photogrammetry and remote sensing. *International Archives of Photogrammetry, Remote Sensing and Spatial Information Sciences*, **37(B1)**, 1201–1206.
- Conrad, C., Fritsch, S., Zeidler, J., Rücker, G., & Dech, S.** (2010). Per-field irrigated crop classification in arid Central Asia using SPOT and ASTER data. *Remote Sensing*, **2(4)**, 1035–1056.
- Dandois, J. P., & Ellis, E. C.** (2013). High spatial resolution three-dimensional mapping of vegetation spectral dynamics using computer vision. *Remote Sensing of Environment*, **136**, 259–276.
- Dawson, I. K., Vinceti, B., Weber, J. C., Neufeldt, H., Russell, J., Lengkeek, A. G., ... & Jamnadass, R.** (2011). Climate change and tree genetic resource management: maintaining and enhancing the productivity and value of smallholder tropical agroforestry landscapes. A review. *Agroforestry Systems*, **81(1)**, 67-78.
- DEAR.** (2005). *Charcoal burning in the Kintampo Districts: Policies, environment and livelihood issues*. Accra, Ghana.
- De-Miguel, S., Mehtätalo, L., & Durkaya, A.** (2014). Developing generalized, calibratable, mixed-effects meta-models for large-scale biomass prediction. *Canadian journal of forest research*, **44(6)**, 648-656.
- Eisenbeiss, H.** (2009). *UAV photogrammetry*.

- ETH Zurich, Switzerland.
- Fatoyinbo, T. E., & Simard, M.** (2013). Height and biomass of mangroves in Africa from ICESat/GLAS and SRTM. *International Journal of Remote Sensing*, 34(June 2015), 668–681. <http://doi.org/10.1080/01431161.2012.712224>
- Fatoyinbo, T. E., Simard, M., Washington-Allen, R. a., & Shugart, H. H.** (2008). Landscape-scale extent, height, biomass, and carbon estimation of Mozambique's mangrove, forests with Landsat ETM+ and Shuttle Radar Topography Mission elevation data. *Journal of Geophysical Research: Biogeosciences*, 113, 1–13. <http://doi.org/10.1029/2007JG000551>
- Feldpausch, T. R., Lloyd, J., Lewis, S. L., Brienen, R. J., Gloor, M., Monteagudo Mendoza, A., & Alexiades, M.** (2012). Tree height integrated into pantropical forest biomass estimates. *Biogeosciences*, 3381–3403.
- Fernández-Landa, A., Navarro, J. A., Condes, S., Algeet-Abarquero, N., & Marchamalo, M.** (2017). High resolution biomass mapping in tropical forests with LiDAR-derived Digital Models: Poás Volcano National Park (Costa Rica). *iForest-Biogeosciences and Forestry*, 10(1), 259.
- Foody, G. M., Boyd, D. S., & Cutler, M. E. J.** (2003). Predictive relations of tropical forest biomass from Landsat TM data and their transferability between regions. *Remote Sensing of Environment*, (85), 463–474. [https://doi.org/10.1016/S0034-4257\(03\)00039-7](https://doi.org/10.1016/S0034-4257(03)00039-7)
- Forestry Commission.** (2012). *National Forest Plantation Development Programme Annual Report*. Accra, Ghana.
- Forzieri, G., Feyen, L., Cescatti, A., & Vivoni, E. R.** (2014). Spatial and temporal variations in ecosystem response to monsoon precipitation variability in southwestern North America. *Journal of Geophysical Research: Biogeosciences*, 119(10), 1999–2017. <https://doi.org/10.1002/2014JG002710>
- Ghana Statistical Service.** (2014). *District Analytical Report Kintampo North District*. Accra, Ghana.
- Gonzalez-Alonso, F., Merino-De-Miguel, S., Roldan-Zamarron, A., Garcia-Gigorro, S., & Cuevas, J.** (2006). Forest biomass estimation through NDVI composites. The role of remotely sensed data to assess Spanish forests as carbon sinks. *International Journal of Remote Sensing. International Journal of Remote Sensing*, 27, 5409–5415. <https://doi.org/10.1080/01431160600830748>
- Goodwin, A. N.** (2004). Measuring tall tree heights from the ground. *Tasforests*, 15, 85–98.
- Jucker, T., Caspersen, J., Chave, J., Antin, C., Barbier, N., Bongers, F., Dalponte, M., van Ewijk, K.Y., Forrester, D.I., Haeni, M. & Higgins, S.I.,** 2017. Allometric equations for integrating remote sensing imagery into forest monitoring programmes. *Global change biology*, 23(1), pp.177-190.
- Karpina, M., Jarzabek-Rychard, M., Tymków, P., & Borkowski, A.** (2016). UAV-Based Automatic Tree Growth Measurement For Biomass Estimation. *ISPRS -International Archives of Photogrammetry and Remote Sensing Spatial Information Sciences*, XLI(July), 685–688. <https://doi.org/10.5194/isprsarchives-XLI-B8-685-2016>
- King, D. A., & Clark, D. A.** (2011). Allometry of emergent tree species from saplings to above-canopy adults in a Costa Rican rain forest. *Journal of Tropical Ecology*, 27(6),

- 573–579.
- Kleinbaum, D. G., Kupper, L. L., & Muller, K. E.** (1988). *Applied Regression Analysis and Other Multivariate Methods: Student's Partial Solutions Manual*. PWS-Kent.
- Korning, J., and Thomsen, K.** (1994). A new method for measuring tree height in tropical rain forest. *Journal of Vegetation Science*, **5**(1), 139–140.
- Lagomasino, D., Fatoyinbo, T., Lee, S., Feliciano, E., Trettin, C., & Simard, M.** (2016). A comparison of mangrove canopy height using multiple independent measurements from land, air, and space. *Remote Sensing*, **8**(4), 324.
- Lim, Y.S.; La, P.H., Park, J.S., Lee, M.H., Pyeon, M.W., & Kim, J.I.** (2015) Calculation of Tree Height and Canopy Crown from Drone Images Using Segmentation. *J. Korean Soc. Surv. Geod. Photogramm. Cartogr.*, **33**, 605–614.
- Lisein, J., Pierrot-Deseilligny, M., Bonnet, S., & Lejeune, P.** (2013). A Photogrammetric Workflow for the Creation of a Forest Canopy Height Model from Small Unmanned Aerial System Imagery. *Forests*, **4**, 922–944.
- Lopez-Serrano, P. M., Lopez-Sanchez, C. A., Diaz-Varela, R. A., Corral-Rivas, J. J., Solis-Moreno, R., Vargas-Larreta, B., & Alvarez-Gonzalez, J. G.** (2015). Estimating biomass of mixed and uneven-aged forests using spectral data and a hybrid model combining regression trees and linear models. *iForest-Biogeosciences and Forestry*, **9**(2), 226–234. <https://doi.org/10.3832/ifor1504-008>
- Mate, R., Johansson, T., & Siteo, A.** (2014). Biomass equations for tropical forest tree species in Mozambique. *Forests*, **5**(3), 535–556.
- Mendoza-Ponce, A., & Galicia, L.** (2010). Aboveground and belowground biomass and carbon pools in highland temperate forest landscape in Central Mexico. *Forestry*, **83**(5), 497–506.
- Meroni, M., Rembold, F., Verstraete, M. M., Gommès, R., Schucknecht, A., & Beye, G.** (2014). Investigating the relationship between the inter-annual variability of satellite-derived vegetation phenology and a proxy of biomass production in the Sahel. *Remote Sensing*, **6**(6), 5868–5884.
- Mi Sun, P., & Yeo-Chang, Y.** (2013). Legal institutions for enhancing and protecting forests as a carbon sink in Japan and the Republic of Korea. *Forest Science and Technology*, **9**(2), 72–80.
- Pabi, O.** (2007). Understanding land-use/cover change process for land and environmental resources use management policy in Ghana. *GeoJournal*, **68**(4), 369–383.
- Pargal, S., Fararoda, R., Rajashekar, G., Balachandran, N., Réjou-Méchain, M., Barbier, N., & Coutron, P.** (2017). Inverting Aboveground Biomass–Canopy Texture Relationships in a Landscape of Forest Mosaic in the Western Ghats of India Using Very High Resolution Cartosat Imagery. *Remote Sensing*, **9**(3), 228.
- Rutishauser, E., Noor'an, F., Laumonier, Y., Halperin, J., Hergoualc'h, K., & Verchot, L.** (2013). Generic allometric models including height best estimate forest biomass and carbon stocks in Indonesia. *Forest Ecology and Management*, **307**, 219–225.
- Samanta, A., Knyazikhin, Y., Xu, L., Dickinson, R.E., Fu, R., Costa, M. H., Saatchi, S.S., Nemani, R.R., & Myneni, R.B.** (2012). Seasonal changes in leaf area of Amazon forests from leaf flushing and abscission. *Journal of Geophysical*

- Research: Biogeosciences*, **117**: G01015.
- Yelsang, F. D.** (2013). Agricultural Land Use Conflict between Landlords and Migrant Farmers in Ghana: An Examination of Issues Affecting Dagara Migrants in the Brong Ahafo Region. *European Scientific Journal*, **9(29)**.
- Zarco-Tejada, P. J., Diaz-Varela, R., Angileri, V., & Loudjani, P.** (2014). Tree height quantification using very high resolution imagery acquired from an unmanned aerial vehicle (UAV) and automatic 3D photo-reconstruction methods. *European Journal of Agronomy*, **55**, 89–99.
- Zhang, H., Zhou, L. G., Chen, M. N., & Ma, W. C.** (2011). Land use dynamics of the fast-growing Shanghai Metropolis, China (1979–2008) and its implications for land use and urban planning policy. *Sensors*, **11(2)**, 1794–1809.
- Zhao, M., & Running, S. W.** (2010). Drought-induced reduction in global terrestrial net primary production from 2000 through 2009. *Science*, **329(5994)**, 940–943. <https://doi.org/10.1126/science.1192666>